bioRxiv preprint doi: https://doi.org/10.1101/242768; this version posted January 4, 2018. The copyright holder for this preprint (which was not certified by peer review) is the author/funder. All rights reserved. No reuse allowed without permission.

Title: Asymmetric histone incorporation during DNA replication in *Drosophila* male germline stem cells

Authors: Matthew Wooten[1], Zehra Nizami[*,2], Xinxing Yang[*,3], Jonathan Snedeker[*,1], Rajesh Ranjan[*,1], Jee Min Kim[1], Elizabeth Urban[1], Vuong Tran[1,4], Jackson Buss[3,5], Joseph Gall[2], Jie Xiao[3], Xin Chen[1,#]

*: equal contribution

[#]: Correspondence to and Lead contact: Xin Chen, Ph.D., Department of Biology, 3400 North Charles Street, The Johns Hopkins University, Baltimore, MD 21218-2685, USA. Tel: 410-516-4576; Fax: 410-516-5213; Email: xchen32@jhu.edu

Affiliations:

[1] Department of Biology, The Johns Hopkins University, Baltimore, MD 21218, USA

[2] Carnegie Institution for Science, Department of Embryology, Baltimore, MD 21218, USA

[3] Department of Biophysics and Biophysical Chemistry, Johns Hopkins University School of Medicine, Baltimore, MD 21205, USA

[4] Current address: 5029 11th Ave. NE, #303, Seattle, WA 91805

[5] Current address: Department of Microbiology and Immunobiology, Harvard Medical School, Boston, MA 02115, USA

bioRxiv preprint doi: https://doi.org/10.1101/242768; this version posted January 4, 2018. The copyright holder for this preprint (which was not certified by peer review) is the author/funder. All rights reserved. No reuse allowed without permission.

Running Title: DNA replication establishes asymmetric epigenomes

SUMMARY

Many stem cells undergo asymmetric division to produce both a self-renewing stem cell and a differentiating daughter cell. We previously reported that in male *Drosophila* germline stem cells (GSCs), preexisting (old) histone H3 is segregated to the self-renewed stem cell, whereas the daughter incorporates newly synthesized (new) H3. Here, we show that histone H4 is likewise segregated asymmetrically, while histones H2A and H2B are segregated symmetrically. Using superresolution imaging, we visualize spatially separable old and new H3 distributions in interphase GSC nuclei and on isolated replicating chromatin fibers. Furthermore, using both superresolved chromatin fibers and proximity ligation assay, we demonstrate that old H3 are preferentially retained on the leading strand while new H3 preferentially associate with the lagging strand. Finally, using a dual nucleoside analog incorporation assay, the temporal separation between leading strand and lagging strand synthesis is detectable. Together, these results demonstrate that the spatial and temporal asymmetries inherent to DNA replication may serve to bias histone incorporation, suggesting an unappreciated role for DNA replication in asymmetrically dividing cells.

bioRxiv preprint doi: https://doi.org/10.1101/242768; this version posted January 4, 2018. The copyright holder for this preprint (which was not certified by peer review) is the author/funder. All rights reserved. No reuse allowed without permission.

INTRODUCTION

One of the most fundamental questions in developmental biology concerns how cells with identical genomes differentiate into distinct cell types. In the process of cell fate specification, epigenetic mechanisms play important roles by altering chromatin structure and gene expression patterns while preserving primary DNA sequences. One important context for understanding cell fate specification is in asymmetric cell division (ACD), where the two daughter cells establish different cell fates following a single division. ACD has been characterized in multiple systems where it has crucial contributions to generate cells with distinct fates in development, homeostasis, and tissue regeneration (Betschinger and Knoblich, 2004; Clevers, 2005; Inaba and Yamashita, 2012; Morrison and Kimble, 2006). Stem cells, in particular, often use ACD to give rise to one daughter cell capable of self-renewal and another daughter cell capable of differentiation. Previous studies have demonstrated that epigenetic mechanisms play crucial roles in maintaining stem cell fate, as well as specifying the cell fate of the differentiating daughter (Atlasi and Stunnenberg, 2017; Avgustinova and Benitah, 2016; Liu et al., 2016). However, many key questions remain concerning how stem cells and differentiating daughter cells might establish different epigenomes following ACD, such that the stem cell retains the same epigenetic memory through many divisions while repeatedly producing differentiating daughter cells that carry distinct epigenomes poised for cellular differentiation.

The *Drosophila* male germline stem cell (GSC) system provides a model to investigate the fundamental molecular and cellular mechanisms underlying ACD (Fuller and Spradling, 2007). Previously, using a dual-color strategy to label preexisting (old) *versus* newly synthesized (new) histones, we reported that the old histone H3 is selectively segregated to the GSC, whereas

bioRxiv preprint doi: https://doi.org/10.1101/242768; this version posted January 4, 2018. The copyright holder for this preprint (which was not certified by peer review) is the author/funder. All rights reserved. No reuse allowed without permission.

the new H3 is enriched in the gonialblast (GB) committed for differentiation (Tran et al., 2012). H3 asymmetry is distinguished through differential phosphorylation at the Thr 3 residue of H3 (H3T3P), followed by specific recognition and segregation during GSC mitosis. Mis-regulation of this key phosphorylation leads to randomized H3 inheritance patterns, as well as severe GSC loss and progenitor germ cell differentiation defects (Xie et al., 2015). Together, these studies provide the *in vivo* evidence showing that stem cells may selectively retain preexisting histones as a means to help regulate stem cell identity, whereas the differentiating daughter cell may inherit predominantly new histone to prepare for proper differentiation.

Our previous work has demonstrated that while H3 shows asymmetric inheritance patterns during GSC division, the H3 variant H3.3 does not (Tran et al., 2012). Because H3 is incorporated during DNA replication, while H3.3 is deposited in a DNA replication-independent manner (Ahmad and Henikoff, 2002b), we hypothesize that DNA replication may play an important role in establishing H3 asymmetry, in preparation for partitioning epigenetic information differentially during the subsequent ACD (Tran et al., 2013; Xie et al., 2017) .

At its most fundamental level, DNA replication duplicates genetic material in the mother cell so that the two daughter cells inherit the identical genome after mitosis. Because DNA polymerase can only synthesize the new strand in a 5'→ 3' direction, DNA replication is an intrinsically asymmetric process, as the leading strand is synthesized continuously (Bessman et al., 1956; Bessman et al., 1958; Kornberg et al., 1989; Lehman et al., 1958) whereas the lagging strand is synthesized in short, discontinuous segments known as Okazaki fragments (Balakrishnan and Bambara, 2013; Okazaki et al., 1968; Sakabe and Okazaki, 1966). Recently, using real-time single-molecule analysis with bacterial DNA as a template *in vitro*, it has been

bioRxiv preprint doi: https://doi.org/10.1101/242768; this version posted January 4, 2018. The copyright holder for this preprint (which was not certified by peer review) is the author/funder. All rights reserved. No reuse allowed without permission.

shown that the syntheses of the leading strand and lagging strand are uncoupled and stochastic at single molecule level. Even though the overall processivity of the replisome is kept, individual polymerization on leading strand *versus* lagging strand could vary independently in a large range (Graham et al., 2017). This finding challenges the long-held dogma that the synthesis of the leading and lagging strands must be synchronized with the same and determined speed and hence may offer a molecular mechanism for other asymmetries to be established at the replication fork.

In eukaryotic cells, just as DNA must be duplicated *via* replication, chromatin must likewise be established on both strands during and after replication. Accordingly, the bulk of canonical histones are synthesized and incorporated during DNA replication. Old histones incorporated in nucleosomes on the parental DNA must be disassembled ahead of the replication fork and reassembled onto one of the two new double-stranded DNA (dsDNA) templates that now exist in the wake of the fork (McKnight and Miller, 1977; Sogo et al., 1986). Although the process of new histone incorporation onto the DNA has been well studied, how old histones are recycled during DNA replication is less clear (Burgess and Zhang, 2013). Previous *in vitro* biochemical studies have shown that old histones can display a strand preference during recycling events in multiple systems (Leffak et al., 1977; Riley and Weintraub, 1979; Roufa and Marchionni, 1982; Seale, 1976; Seidman et al., 1979; Weintraub, 1976). However, the mode of histone incorporation has not been systematically studied in any multicellular organism *in vivo*. Characterizing the mechanisms of histone incorporation mode during DNA replication in cells under their physiological condition is critical to our understanding of epigenetic regulation in animal development and various diseases, including cancer and tissue dystrophy [reviewed in (Snedeker et al., 2017)].

bioRxiv preprint doi: https://doi.org/10.1101/242768; this version posted January 4, 2018. The copyright holder for this preprint (which was not certified by peer review) is the author/funder. All rights reserved. No reuse allowed without permission.

RESULTS

Old histone H4 showed asymmetric inheritance pattern during *Drosophila* male GSC asymmetric division

Using a heat shock-controlled switching system to label old histone with GFP (green fluorescent protein) and new histone with mKO (monomeric Kusabira Orange fluorescent protein) (Figure S1A), we explored the inheritance pattern for all canonical histones following the asymmetric division of male *Drosophila* GSCs. The distributions of old histone (GFP) and new histone (mKO) were measured following the second mitosis after heat shock-induced genetic switch (Figure 1A) (Tran et al., 2012). Since mitotic GSCs account for less than 2% of the total population of GSCs (Sheng and Matunis, 2011; Tran et al., 2012; Yadlapalli et al., 2011; Yadlapalli and Yamashita, 2013), post-mitotic GSC-GB pairs derived from the asymmetric division GSCs were first used to visualize and quantify histone inheritance patterns in fixed images (Tran et al., 2012; Xie et al., 2015) (EXPERIMENTAL PROCEDURES). For H4, we found that old H4-GFP was enriched (~ 3.3-fold) in the GSCs (Figures 1B and 1D), as reported previously for old H3 (Tran et al., 2012; Xie et al., 2015). New H4-mKO was symmetrically distributed between GSCs and GBs (Figures 1B and 1D). Presence of newly synthesized H4-mKO in both nuclei of the GSC-GB pair was consistent with the fact that both cells underwent S phase after the second mitosis following heat shock, as indicated by ~ 30-minute EdU (5-ethynyl-2'-deoxyuridine) incorporation (Figures 1A and 1B). By contrast, such an asymmetric old H4 inheritance pattern was not observed in S-phase spermatogonial pairs after symmetrical cell division (Figures 1C and 1D).

We next examined the H4 segregation pattern in mitotic GSCs. In both anaphase (Figure 1E) and telophase (Figure 1F) GSCs, old H4-GFP also showed asymmetric segregation patterns.

bioRxiv preprint doi: https://doi.org/10.1101/242768; this version posted January 4, 2018. The copyright holder for this preprint (which was not certified by peer review) is the author/funder. All rights reserved. No reuse allowed without permission.

Because mitotic GSCs are significantly under-represented in fixed testis samples, we replaced the GFP with EGFP (enhanced GFP) for old H4 and mKO with mCherry for new H4 (Figure S1A), in order to facilitate visualizing signals in live cell imaging to obtain more mitotic GSCs. In telophase GSCs, old H4-EGFP preferentially segregated toward the GSC side (Figure 1G, Movies S1), similar to what was observed in fixed mitotic GSCs. New H4-mCherry segregation pattern was symmetric (Figure 1G, Movies S2). Furthermore, live mitotic spermatogonial cells showed symmetric segregation pattern for both old and new H4 (Figure 1G, Movies S3-S4). These results established that old H4 segregated asymmetrically during ACD, similar to H3.

Histones H2A, H2B and H1 showed symmetric inheritance patter during *Drosophila* male GSC asymmetric division

Next, we characterized the inheritance patterns of the rest of the canonical histones: H2A, H2B, and the linker histone H1 (Figure S1A). Using a similar heat shock-induced switching scheme (Figure 1A), we found that old and new H2A (Figures 2A and 2C) as well as old and new H2B (Figures 2B and 2D) showed symmetric inheritance patterns in post-mitotic GSC-GB pairs. Additionally, both H2A (Figure 2C) and H2B (Figure 2D) displayed symmetric old and new histone inheritance patterns in post-mitotic spermatogonial pairs. Further investigation of mitotic GSCs at either anaphase or telophase confirmed this globally symmetric inheritance pattern for both H2A (Figure 2E) and H2B (Figure 2F). Additionally, live cell imaging of H2A in both asymmetrically dividing GSCs and symmetrically dividing spermatogonial cells showed largely symmetric distributions of old and new histones (Figure 2G, Movies S5-S6). Finally, the linker histone H1 also showed globally symmetric inheritance pattern in post-mitotic GSC-GB pairs (Figure S1B).

bioRxiv preprint doi: https://doi.org/10.1101/242768; this version posted January 4, 2018. The copyright holder for this preprint (which was not certified by peer review) is the author/funder. All rights reserved. No reuse allowed without permission.

Overall, histones H3 and H4 showed significantly greater asymmetric distributions in asymmetrically dividing GSCs when compared to H2A and H2B. These findings demonstrated that even though H3, H4, H2A and H2B are all incorporated in a replication-dependent manner, different histones display different dynamics in terms of their incorporation at the replication fork and/or different stabilities and exchange rates post-replication. Previous biochemical studies have established that H3 and H4 are incorporated as a tetramer $(H3\text{-}H4)_2$, while H2A and H2B are incorporated as dimers (Annunziato et al., 1982; Jackson, 1988; Jackson and Chalkley, 1981a, b; Katan-Khaykovich and Struhl, 2011; Russev and Hancock, 1981; Xu et al., 2010). Because H4 is incorporated as a tetramer with H3, the similar asymmetric inheritance pattern of old H3 and H4 suggested that the preexisting $(H3\text{-}H4)_2$ tetramers did not split and were inherited as a whole unit, consistent with previous reports (Xu et al., 2010). Conversely, H2A and H2B are incorporated as dimers and exhibit much more dynamic behavior compared to $(H3\text{-}H4)_2$ tetramers (Kimura, 2005). To our current knowledge, H3 and H4 have the majority of known post-translational modifications and may act as the major epigenetic information carriers (Allis and Jenuwein, 2016; Kouzarides, 2007; Young et al., 2010).

Superresolution imaging revealed distinct H3 *versus* H3.3 patterns in interphase GSCs

Our previous studies have demonstrated that H3, but not H3.3, are asymmetrically inherited during asymmetric division of GSCs (Tran et al., 2012; Xie et al., 2015). Because H3 is incorporated during S-phase whereas H3.3 is incorporated in a replication-independent manner, it is likely that old and new H3 are differentially incorporated into distinct sister chromatids during DNA replication. As such, H3 and H3.3 may have already exhibited differential distributions in interphase cells following the first mitosis after heat shock, before the second

bioRxiv preprint doi: https://doi.org/10.1101/242768; this version posted January 4, 2018. The copyright holder for this preprint (which was not certified by peer review) is the author/funder. All rights reserved. No reuse allowed without permission.

mitosis (Figure 1A). To facilitate the quantitative comparison between H3 and H3.3 distribution patterns on un-condensed chromosomes in interphase GSCs, we re-labeled old H3 or H3.3 with a photo-switchable GFP Dronpa, new H3 or H3.3 with a photo-activatable RFP PAmCherry (Figures S2A-S2B), and visualized their distributions using single molecule localization based two-color superresolution imaging (Betzig et al., 2006). In interphase GSCs, we observed heterogeneously localized regions of old and new histones for both H3 (Figure 3A) and H3.3 (Figure 3D); these distribution patterns were different from a homogenous, random distribution expected from the same cells (Figures 3B-C and 3E-F), suggesting that the underlying chromosome distribution was not uniform. Coordinate-based cross-correlation analysis (Veatch et al., 2012) between Dronpa-labeled (old) and PAmCherry-labeled (new) histones revealed that the correlation value between the localizations of H3.3-Dronpa and H3.3-PAmCherry was largely constant and remained significantly higher than that of H3 at all distance up to ~ 600 nm (Figure 3G, compare the red curve with the black curve), suggesting that on this length scale old and new H3.3 colocalized with each other to a higher degree than H3. Interestingly, at short distances (< 50 nm), H3-Dronpa and H3-PAmCherry showed anti-correlation indicated by negative correlation values (Figure 3G, zoom-in view), and only became weakly correlated at longer distances. These results suggested that old and new H3 were already differentially positioned with respective to each other in interphase GSCs compared to H3.3, consistent with our hypothesis that old and new H3 are differentially incorporated during S phase while H3.3 is not.

Distinct patterns between old and new histones on chromatin fibers

bioRxiv preprint doi: https://doi.org/10.1101/242768; this version posted January 4, 2018. The copyright holder for this preprint (which was not certified by peer review) is the author/funder. All rights reserved. No reuse allowed without permission.

To test the hypothesis that old and new H3 are differentially incorporated during DNA replication more directly, we adapted the chromatin fiber technique (Ahmad and Henikoff, 2002a; Blower et al., 2002; Cohen et al., 2009; Nieminuszczy et al., 2016) to extract EdU pulse-labeled (30 minutes) chromosomal DNA with associated proteins, including histones, from early-stage germ cells in *Drosophila* testis expressing *nanos>histone* transgenes (Van Doren et al., 1998). By spreading chromatin fibers on glass slides, we could unambiguously identify the distribution of old and new histones along replicating and newly replicated sister chromatids outside the confines of the nucleus.

We stained extracted chromatin fibers using YOYO-3, a highly fluorescent dsDNA intercalating dye, and compared with EdU-labeled regions along the fibers. Using confocal microscopy, we observed discrete fragments of EdU localized along the length of YOYO-3-labeled ($YOYO^+$) chromatin fibers (Figure S3). Isolated EdU fragments showed an average size of 2μm on chromatin fibers (Figure S5). Intriguingly, EdU-labeled regions (EdU^+) largely coincided with bright but not dim $YOYO^+$ regions and also with proliferating cell nuclear antigen (PCNA), a key protein involved in the process of DNA replication (Figure S3). Using STimulated Emission Depletion (STED) superresolution microscopy (Hell and Wichmann, 1994), which offers higher spatial resolution (~ 80 nm) than confocal microscopy, bright $YOYO^+$ regions resolved into closely paired doublets whereas dim $YOYO^+$ regions only showed as singlets (Figure 4A). The separation between two fibers in a doublet ranged from 80 nm to 2000 nm, similar to what was observed in replication bubbles in extracted chromosomal DNAs from *Drosophila* embryonic cells, previously visualized using electron microscopy (McKnight and Miller, 1977). The resolved fibers (singlets and individual ones in doublets) appeared to be ~ 70-100 nm wide in both STED and single-molecule localization based superresolution imaging

bioRxiv preprint doi: https://doi.org/10.1101/242768; this version posted January 4, 2018. The copyright holder for this preprint (which was not certified by peer review) is the author/funder. All rights reserved. No reuse allowed without permission.

(Figure S4A-S4B) (Rust et al., 2006); the latter had a higher spatial resolution (13.6nm, Figures S2C-S2D) than STED. Because the width of ~ 70-100nm was significantly larger than what would be expected for naked, single dsDNA strand under the same spatial resolution (Watson and Crick, 1953), and that bundled chromatins consisted of multiple dsDNA strands appeared wider and with different morphology under the same imaging condition (Figure S4C), these singlet fibers likely represented single dsDNA strands wrapped with nucleosomes and other chromatin associated proteins.

Using EdU as a marker to visualize newly synthesized DNA under STED microscopy, we quantified and found that a significantly higher percentage of unlabeled (EdU^-) fibers resolved into singlets (Figure 4B) than doublets (71.4% *vs.* 28.6%), and a significantly higher percentage of labeled (EdU^+) fibers resolved into doublets (Figure 4C) than singlets (64.3% *vs.* 35.7%) (Figure 4D). These results suggested that singlet fibers likely represented un-replicated dsDNA strands while doublet fibers likely represented replicated sister chromatids labeled during the 30-minute EdU pulsing. The 28.6% EdU^- doublets likely represented replicated sister chromatids whose synthesis occurred outside the 30-minute window of EdU incorporation; while the 35.7% EdU^+ singlets could have resulted from the physical separation of the two previously cohesed sister chromatids during the process of fiber separation (EXPERIMENTAL PROCEDURES), or tightly cohesed regions that could not be resolved even with superresolution microscopy. Of note, these two percentages were much lower than the other two categories (i.e. EdU-positive doublet fibers and EdU-negative single fiber) ($P < 0.05$, Figure 4D), suggesting that our method largely preserved replicating or replicated sister chromatids.

Next, to analyze the distribution of old and new histones along sister chromatids, we isolated chromatin fibers from early-stage germ cells expressing labeled old and new H3 or H3.3

bioRxiv preprint doi: https://doi.org/10.1101/242768; this version posted January 4, 2018. The copyright holder for this preprint (which was not certified by peer review) is the author/funder. All rights reserved. No reuse allowed without permission.

(*nanos>H3 or H3.3*). Doublet fibers ranging in size from just under 1μm to over 10μm could be found, which showed significant asymmetry between old H3-GFP and new H3-mKO (Figures 4E and 4F). By contrast, old H3.3-GFP and new H3.3-mKO showed relatively even distribution along the two parallel fibers in doublets (Figure 4G).

Quantification of old and new histone distributions on chromatin fibers revealed a wide range of histone distribution patterns for both H3 and H3.3 (Figure 4H). Fibers labelled with H3 and H3.3 could be found with relatively symmetric levels of old histone (ratio < 2) and asymmetric levels of old histone (ratio > 2). Importantly, H3 fibers showed a significantly higher incidence of old H3 asymmetry than did old H3.3 (Figure 4H, $P < 0.05$). On average, H3 fibers showed a 2.34±0.20 (avg. ± s.e.) ratio of old H3 between sister chromatids, with 27 out of 56 fiber segments showing > 2-fold difference of old H3. By comparison, H3.3 fibers showed a 1.77±0.10 ratio of old H3.3 between sister chromatids with only 15 out of 56 fiber segments showing > 2-fold difference of old H3.3. On the other hand, new histones showed a more symmetric distribution for both H3 and H3.3 chromatin fibers. On average H3 fibers showed a 1.47±0.17 ratio of new H3 between sister chromatids, with 15 out of 56 fiber segments showing > 2-fold difference of new H3. By comparison, H3.3 fibers showed a 1.25±0.09 ratio of new H3.3 between sister chromatids, with 12 out of 56 fiber segments showing > 2-fold difference of new H3.3. In summary, while new histone distribution appeared to show similar patterns in H3 and H3.3 chromatin fibers, old H3 showed a more pronounced asymmetric pattern between sister chromatids than did old H3.3 (Figure 4H). Consistent with previous PALM data, these data suggested that old and new H3 showed more frequent separation than did old and new H3.3.

bioRxiv preprint doi: https://doi.org/10.1101/242768; this version posted January 4, 2018. The copyright holder for this preprint (which was not certified by peer review) is the author/funder. All rights reserved. No reuse allowed without permission.

Distinct distribution between old and new H3 with strand-enriched DNA replication machinery component

As H3 is mainly incorporated during DNA replication, we tested whether old H3 asymmetry correlated in any way with strand-enriched DNA replication machinery components. We imaged old H3-GFP and new H3-mKO on isolated chromatin fibers immunostained for PCNA, a key replication component enriched at the lagging strand (Yu et al., 2014). We found that indeed PCNA was enriched on one of the fibers in doublets (Figure 5A), with an average enrichment ratio of ~ 2 between sister chromatids (Figure 5B), consistent with previous report (Yu et al., 2014).

We then examined doublet fibers that had pronounced PCNA asymmetry (enrichment ratio > 2-fold), which most likely represented lagging strands undergoing active synthesis. We found that old H3-GFP showed a significantly greater level of enrichment on the PCNA-depleted sister chromatid ($P<0.05$), whereas new H3-mKO showed a significantly higher level of enrichment on the PCNA-enriched sister ($P<0.05$, Figure 5C). Taken together, these results indicated that during DNA replication, old H3 was preferentially incorporated towards the leading strand whereas new H3 was preferentially incorporated onto the lagging strand.

Proximity Ligation Assay revealed strand preference between old and new H3 during replication coupled nucleosome assembly

While the chromatin fiber technique offered many advantages in terms of understanding protein distribution on sister chromatids, the process of lysing the nuclei made retaining information related to cell identity almost impossible. To further explore the question of histone inheritance at the replication fork in a cell-type-specific manner, we used CRISPR/Cas9-mediated genome

bioRxiv preprint doi: https://doi.org/10.1101/242768; this version posted January 4, 2018. The copyright holder for this preprint (which was not certified by peer review) is the author/funder. All rights reserved. No reuse allowed without permission.

editing (Horvath and Barrangou, 2010; Wright et al., 2016) to tag the leading strand-specific DNA polymerase ε (Pol ε) and lagging strand-specific DNA ligase at their corresponding genomic locus using a 3xHA epitope. As Pol ε is specifically enriched upon the leading strand whereas DNA ligase is specifically enriched upon the lagging strand, these tagged proteins serve as proxies for the leading strand (Pol-ε-HA) and the lagging strand (Ligase-HA) during DNA replication (Yu et al., 2014). We applied these tagged proteins for an imaging based proximity ligation assay (PLA) to probe the spatial proximity between histones (old *versus* new) and replication components specifically enriched upon either the leading strand (Pol ε) or the lagging strand (Ligase). The PLA method enables positive fluorescence detection if two proteins of interest are in close proximity (< 40 nm), which has been successfully applied in fly embryos (Petruk et al., 2012).

We used antibodies against either old H3 (anti-GFP) or new H3 (anti-mKO) with anti-HA that targeted either Pol ε or ligase for PLA experiments in GSCs. We observed a higher number of PLA fluorescent puncta between ligase and new H3 (mKO, Figure 6A, 26.5 ± 1.7, avg. ± s.e., n = 35 GSCs) than those between ligase and old H3 (GFP, Figure 6B, 18.5 ± 2.5, n = 53; Figure 6E, $P < 0.01$). Conversely, fewer PLA fluorescent puncta were detected between Pol ε and new H3 (mKO, Figure 6C, 9.3 ± 1.1, n = 41) compared to those between Pol ε and old H3 (GFP, Figure 6D, 17.2 ± 1.0, n = 34; Figure 6F, $P<0.01$). These results were consistent with the chromatin fiber experiments, indicating that old H3 preferentially associated with the leading strand whereas new H3 preferentially associated with the lagging strand. Consistent with the lagging strand-specific ligase results, the lagging strand-enriched PCNA also showed more PLA fluorescent puncta with new H3 (mKO, Figure S6, 13.2 ± 1.4, n = 13) than with old H3 (GFP, Figure S6, 6.5 ± 0.8, n = 22; $P < 0.01$).

bioRxiv preprint doi: https://doi.org/10.1101/242768; this version posted January 4, 2018. The copyright holder for this preprint (which was not certified by peer review) is the author/funder. All rights reserved. No reuse allowed without permission.

Interestingly, spermatogonial cells (SGs) showed a less pronounced strand preference for old and new histones when compared to GSCs (Figures 6E and 6F), suggesting that histones may show distinct incorporation mode during DNA replication in these two different staged germ cells. Unlike GSCs, PLA comparing old and new H3 association with Ligase showed no significant differences (Figure 6E). Furthermore, PLA comparing old H3 association with Pol ε showed significant decrease of PLA puncta from GSCs to SGs (17.2 *versus* 12.3; $P < 0.01$). However, PLA comparing new H3 association with Pol ε showed no significant change from GSCs to SGs, leading to a less dramatic difference in old and new histone association with Pol ε in SGs (Figure 6F). Together, these findings suggested that the asymmetry observed at the replication fork during DNA replication became less pronounced as germ cells differentiate, consistent with previous results (Figure 1). These findings further demonstrated that histone distribution patterns showed a cellular specificity not only during mitosis, but also during DNA replication.

Nucleoside analogue incorporation assay showed separable timing of DNA replication

The experiments described above demonstrated that old H3 were preferentially incorporated to the leading strand while the new H3 were preferentially enriched to the lagging strand. One possibility for establishing this differential incorporation pattern could be that the lagging strand replication is delayed relative to the leading strand such that recycled old histones prefer the leading strand as it serves a better substrate for histone incorporation at the fork (Adkins et al., 2017; Dunn and Griffith, 1980). A key consequence of this temporal delay would be that at the time of old histone recycling, the leading strand, by virtue of being fully synthesized and

bioRxiv preprint doi: https://doi.org/10.1101/242768; this version posted January 4, 2018. The copyright holder for this preprint (which was not certified by peer review) is the author/funder. All rights reserved. No reuse allowed without permission.

processed, would provide a more suitable substrate for old H3 recycling than the incompletely synthesized lagging strand.

To investigate this possibility, we compared EdU incorporation patterns between short (10 minutes) and long (> 30 minutes) labeling pulses. We reasoned that if the synthesis of leading and lagging strands is synchronous, both short and long EdU labeling pulses should result in similar labeling density between the two sister chromatids. On the contrary, if there were a temporal asynchrony, short EdU labeling pulses would only label one sister chromatid in a doublet fiber, likely representing the replication of either the leading or lagging strand, but not both at the same time. Consistent with the latter expectation, we observed stretches of EdU^+ singlet fibers (arrow in Figure 7A) interspaced with small stretches of doublets (yellow rectangular in Figure 7A), with short EdU-labeling. By contrast, largely uniform EdU^+ doublet fibers could be detected using long EdU-labeling.

We further validated this asynchronous incorporation pattern using a dual nucleoside analog incorporation scheme—cells were first labeled with a long EdU pulse and then followed with a short BrdU (5-Bromo-2'-deoxyuridine) pulse. As shown in Figure 7C, short BrdU pulse labeling resulted in significantly greater asymmetry than the long EdU pulse labeling: Fibers receiving a 10-minute pulse showed over a two-fold difference in the BrdU intensity between two sister chromatids (2.96±0.41, avg.±s.e., n=40), whereas fibers receiving a pulse of over 30 minutes showed less asymmetry (1.78±0.20, n=38) (P< 0.01, Figure 7D). Taken together, these results indicated that the synthesis of the leading and the lagging strand may not proceed in a simultaneous manner.

DISCUSSION

bioRxiv preprint doi: https://doi.org/10.1101/242768; this version posted January 4, 2018. The copyright holder for this preprint (which was not certified by peer review) is the author/funder. All rights reserved. No reuse allowed without permission.

In this work, we utilized a series of imaging-based approaches to explore whether and how DNA replication plays a role in asymmetric histone inheritance in *Drosophila* male GSCs. Our data demonstrate that preexisting H3 preferentially associate with leading strand while newly synthesized H3 are incorporated into the lagging strand. Additionally, our data suggest that in the *Drosophila* germline, leading strand and lagging strand syntheses are likely asynchronous in time, providing a possible mechanism to bias old H3 and new H3 incorporation at the replication fork, due to the different degree of the double-strandness between the two strands. As such, DNA replication may play a novel, unappreciated role in directing histones incorporation on two identical, replicating DNA strands, and hence setting up epigenetic information differentially on two sister chromatids (Figure 7E).

This study has adapted several technical innovations: We have optimized the chromatin fiber technique and combined it with the superresolution microscopy to visualize sister chromatids, as they are undergoing the processes of DNA replication and replication-coupled nucleosome assembly. Using sequential pulses of the thymidine analogues, temporal replication asynchrony on sister chromatid fibers could be captured and visualized in a spatially separable manner (Figure 7). By combining superresolution imaging of chromatin fibers with the dual-color histone labeling system, we established a novel method to study replication-coupled nucleosome assembly. Studying histone segregation patterns on the single fiber level allowed us to better understand the variability of histone segregation patterns in a wide variety of chromatin contexts (Figure 4). Furthermore, we were able to demonstrate that the strand preference of old and new histones (Figure 5). This information would be difficult to attain by other means in cells. Hence, by combining chromatin fiber preparation with antibody labelling and

bioRxiv preprint doi: https://doi.org/10.1101/242768; this version posted January 4, 2018. The copyright holder for this preprint (which was not certified by peer review) is the author/funder. All rights reserved. No reuse allowed without permission.

superresolution imaging, we were able to directly observe the processes by which sister chromatids are built and acquire epigenetic identity.

It has long been recognized that DNA replication is an inherently asymmetric process. Both the molecular components and temporal order of the synthesis of the leading and lagging strands are distinct. Previous work has demonstrated that many cells overcome this asymmetry by regulating the progression of the replication fork, such that both strands are synthesized concurrently with replication fork progression, leading to simultaneous synthesis of two genetically identical sister chromatids (Alberts et al., 1983; Bermek et al., 2015; Debyser et al., 1994; Hamdan et al., 2009; Lee et al., 1998; Lee et al., 2006; Prelich and Stillman, 1988; Stano et al., 2005; Stengel and Kuchta, 2011; Yao et al., 2009). However, studies perturbing key molecular players involved in DNA replication have shown that it is possible to uncouple these two processes (Kadyrov and Drake, 2002; Yang et al., 2006; Yeeles and Marians). Furthermore, recent single molecule *in vitro* studies have suggested an alternative model, in which each polymerase proceeds in a stochastic manner, such that long gaps (kilobases in length) in sister chromatid synthesis could occur as a result of temporal and spatial separation between leading strand and lagging strand synthesis (Graham et al., 2017). Here, our study presents *in vivo* evidence suggesting that similar mechanisms may be involved in regulating replication fork progression in the *Drosophila* germline. Our data reveal that sister chromatids showed frequent asynchrony in the timing of their respective synthesis and that this asynchrony became much less frequent with long labeling pulses (Figure 7). These findings suggest that asynchronies between leading/lagging strand syntheses were short lived, and that two sisters would eventually achieve symmetric levels of replication if given sufficient time.

bioRxiv preprint doi: https://doi.org/10.1101/242768; this version posted January 4, 2018. The copyright holder for this preprint (which was not certified by peer review) is the author/funder. All rights reserved. No reuse allowed without permission.

Our findings additionally have important implications for understanding epigenetic inheritance, specifically the process of replication-coupled nucleosome assembly. Prior work has demonstrated that nucleosomes which are displaced ahead of the replication fork are recycled almost immediately with extremely high efficiency (Alabert et al., 2015; Verreault, 2003; Worcel et al., 1978). Due to the continuous nature of leading strand synthesis, it has been hypothesized that old histones may preferentially associate with the leading strand during the process of histone recycling (Annunziato, 2013; Snedeker et al., 2017). Accordingly, EM studies of replicating SV40 viral chromosomes have demonstrated that histones tend to associate with the leading strand sooner (~225nt after fork passage) than with the lagging strand (~285nt after fork passage). While large-scale asymmetries in the deposition of histone proteins have been observed experimentally (Riley and Weintraub, 1979; Seale, 1976; Seidman et al., 1979; Sogo et al., 1986; Weintraub, 1976), a majority of studies have demonstrated that on a global scale, old and new histones are associated with the leading and the lagging strands with equal efficiency (Alabert and Groth, 2012; Annunziato, 2013; Jackson and Chalkley, 1981a, 1985). These findings suggest that the fundamental differences between leading strand and lagging strand replication may not be sufficient to bias histone inheritance patterns globally across different cell types. However, this question had not been addressed thoroughly in a multicellular organism in a developmental context. Using superresolution imaging of chromatin fibers in tandem with our dual-color histone labelling system, we have been able to describe a wide range of old and new histone distribution patterns between sister chromatids in the *Drosophila* germline for H3 and H3.3 (Figure 4). Our results suggest that histone segregation patterns had molecular specificity, as on a population-wide level, H3-labelled fibers showed larger and more frequent asymmetric distribution patterns when compared to H3.3-labelled fibers. These findings suggest that

bioRxiv preprint doi: https://doi.org/10.1101/242768; this version posted January 4, 2018. The copyright holder for this preprint (which was not certified by peer review) is the author/funder. All rights reserved. No reuse allowed without permission.

different histones may behave differently during the process of chromatin recycling and maturation. Interestingly, both H3 and H3.3 showed a wide range of symmetries ranging from nearly symmetric (1:1 ratio between sisters) to highly asymmetric (8:1 for H3; 5:1 for H3.3) (Figure 4H). The heterogeneity in histone distribution between sister chromatin fibers suggests that the process of replication-coupled nucleosome assembly was not uniformly regulated throughout the germline. Rather, factors such as cell type and genomic context may play important roles in regulating the distribution of old and new histones at the replication fork. Indeed, results from our PLA studies suggest that the process of histone recycling may be subject to regulation in a cell-type specific manner, as asymmetrically dividing GSCs showed a more pronounced asymmetry at the fork than did symmetrically dividing SGs. Because we could not discern GSC-derived fibers from SG-derived fibers, it is likely that some of the variability seen in fiber data may come from different staged cells. Furthermore, isolated fibers also lack any sort of sequence information. Therefore, it is also possible that different regions of the genome may display different histone incorporation patterns. Further studies using a GSC-specific marker, which is currently unavailable, as well as technologies to decode sequence information of the fibers will be needed to address these questions. Lastly, if replication forks are proceed outward from origins of replication in a bidirectional manner, asymmetries in histone inheritance at the replication fork alone would not be sufficient to explain the global asymmetries in histone inheritance we have observed for H3 and H4. Therefore, we hypothesize that certain mechanisms exist to coordinate replication forks in GSCs to achieve a long-range histone asymmetry between sister chromatids. Understanding how replication proceeds in the GSCs and the molecular mechanisms by which coordination could occur are subjects of our ongoing research.

bioRxiv preprint doi: https://doi.org/10.1101/242768; this version posted January 4, 2018. The copyright holder for this preprint (which was not certified by peer review) is the author/funder. All rights reserved. No reuse allowed without permission.

In summary, our work demonstrates that the intrinsic asymmetries in DNA replication process may help construct sister chromatids enriched with distinct populations of histones. These findings hint at the exciting possibility that DNA replication can be exploited in a cell-type specific manner. While the molecular player(s) responsible for this cell-type-specificity remains unclear, this demonstration of a potential regulatory role for DNA replication represents an important step forward in understanding how DNA replication and replication-coupled nucleosome assembly intersect to regulate distinct epigenetic identities of different cell types.

bioRxiv preprint doi: https://doi.org/10.1101/242768; this version posted January 4, 2018. The copyright holder for this preprint (which was not certified by peer review) is the author/funder. All rights reserved. No reuse allowed without permission.

Figures and Figure Legends:

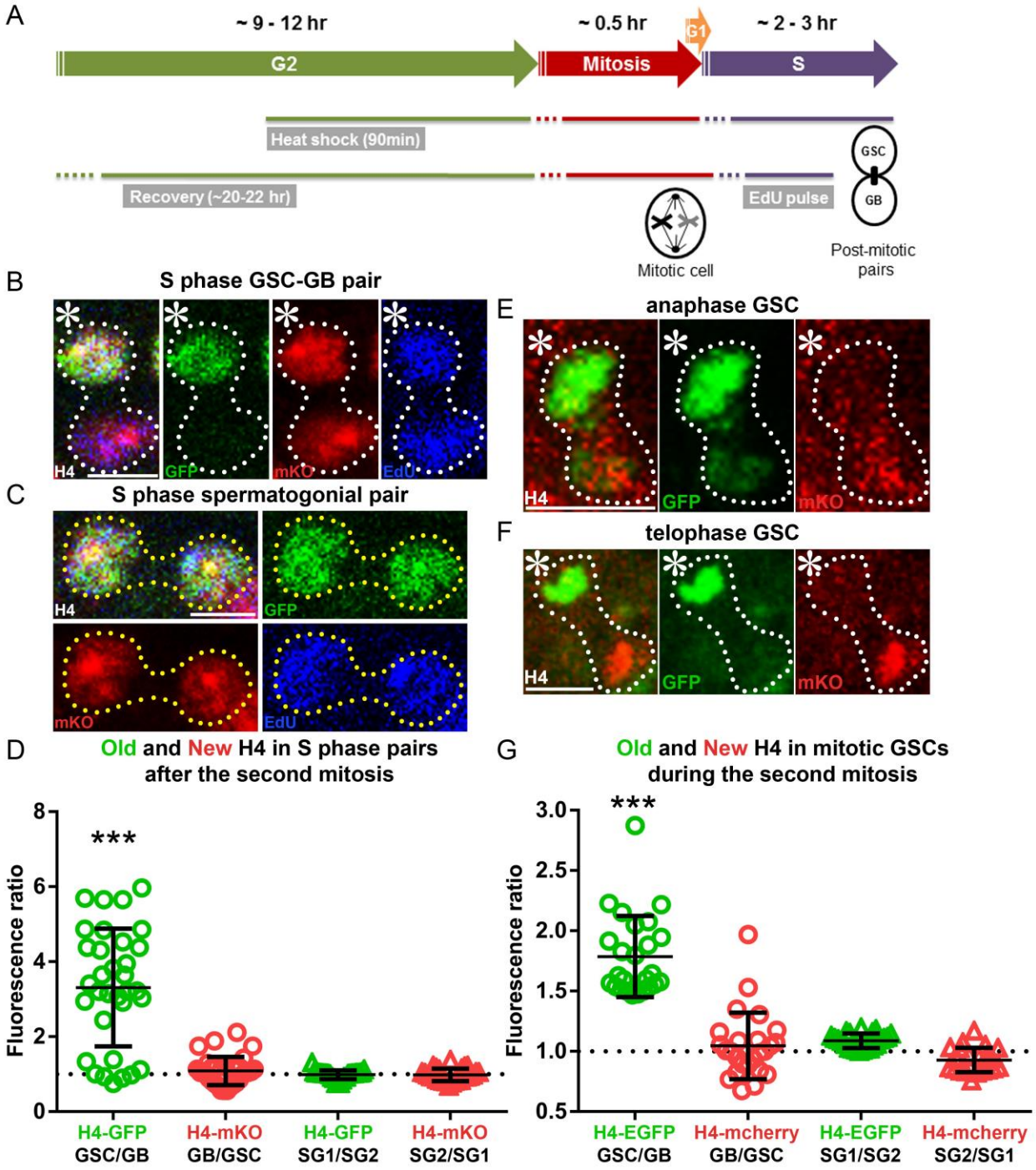

Figure 1: Old histone H4 shows asymmetric distribution during *Drosophila* GSC asymmetric division. (A) A cartoon depicting the experimental design. **(B)** H4 distribution patterns in a post-mitotic GSC-GB pair labeled with EdU (blue): H4-GFP (green) is distributed

bioRxiv preprint doi: https://doi.org/10.1101/242768; this version posted January 4, 2018. The copyright holder for this preprint (which was not certified by peer review) is the author/funder. All rights reserved. No reuse allowed without permission.

asymmetrically towards the GSC whereas H4-mKO (red) distributed more evenly between the GSC and the GB. **(C)** H4 distribution patterns in a post-mitotic spermatogonial cell pair. Both H4-GFP and H4-mKO are symmetrically distributed between the two spermatogonial (SG) nuclei. (**D**) Quantification of H4-GFP and H4-mKO distribution in GSC-GB pairs (n= 31) and SG1-SG2 pairs (n= 23). (**E**) An anaphase GSC showing asymmetric segregation of H4-GFP towards the GSC and H4-mKO towards the GB. (**F**) A telophase GSC showing asymmetric distribution of H4-GFP towards the GSC and H4-mKO towards the GB. (**G**) Quantification of live cell imaging movies showing asymmetric old H4-EGFP segregation patterns in GSCs (n= 25) during the second mitosis after heat shock-induced genetic switch. Differences for new H4 between live cell imaging and fixed samples could result from unincorporated new histones, which had been largely cleared from fixed samples but were likely present in live cells. Similar quantification in mitotic spermatogonial cells (n= 23) showed symmetric patterns. *** $P<$ 0.0001, two-tailed student's *t*-test if average significantly different than 1. Scale bar: 5μm. Asterisk: hub.

bioRxiv preprint doi: https://doi.org/10.1101/242768; this version posted January 4, 2018. The copyright holder for this preprint (which was not certified by peer review) is the author/funder. All rights reserved. No reuse allowed without permission.

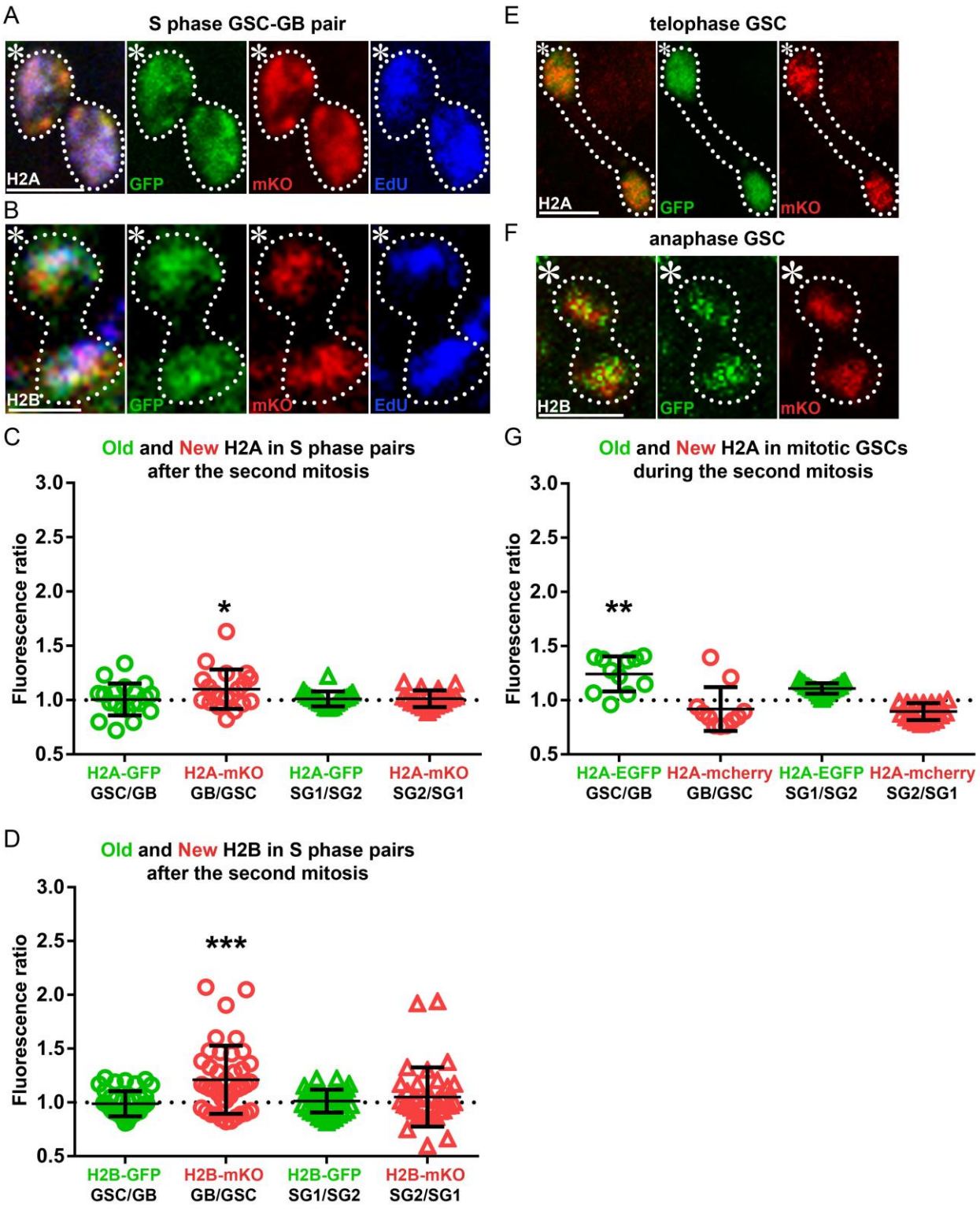

Figure 2: Histones H2A and H2B show symmetric distribution during *Drosophila* GSC asymmetric division. (**A**) Symmetric H2A inheritance pattern in a post-mitotic GSC-GB pair.

bioRxiv preprint doi: https://doi.org/10.1101/242768; this version posted January 4, 2018. The copyright holder for this preprint (which was not certified by peer review) is the author/funder. All rights reserved. No reuse allowed without permission.

(B) Symmetric H2B inheritance pattern in a post-mitotic GSC-GB pair. (**C**) Quantification of H2A-GFP and H2A-mKO distribution in GSC-GB pairs (n= 20) and SG1-SG2 pairs (n= 20). (**D**) Quantification of H2B-GFP and H2B-mKO distribution in GSC-GB pairs (n= 40) and SG1-SG2 pairs (n= 36). (**E**) A telophase GSC showing symmetric segregation of H2A-GFP and H2A-mKO. (**F**) An anaphase GSC showing symmetric segregation of H2B-GFP and H2B-mKO. (**G**) Quantification of live cell imaging movies showing symmetric H2A-EGFP and H2A-mCherry segregation patterns in both mitotic GSCs (n=11) and spermatogonial cells (n=21). *** $P<$ 0.0001, ** $P<$ 0.001, * $P<$ 0.05, two-tailed student's *t*-test if average significantly different than 1. While the majority of H2A and H2B quantifications showed symmetry, certain groups show statistically significant differences from hypothetical value of 1. Interestingly, both new H2A and new H2B show a subtle, but statistically significant enrichment in GB compared to GSC in post-mitotic pairs. It is likely that these differences arised after mitosis, because these differences were not present in mitotic cells based on live cell imaging. Live cell imaging also showed old H2A to have a subtle but statically significant enrichment toward GSC side during asymmetric division of GSCs. These findings suggest that GSCs may selectively retain old H2A, just to a much lesser extent than that retention for either H3 or H4. Additionally, unlike H3 or H4, this asymmetry for old H2A seemed to be short-lived, as analysis of post-mitotic pairs showed a symmetric distribution of old H2A. Scale bar: 5μm. Asterisk: hub.

bioRxiv preprint doi: https://doi.org/10.1101/242768; this version posted January 4, 2018. The copyright holder for this preprint (which was not certified by peer review) is the author/funder. All rights reserved. No reuse allowed without permission.

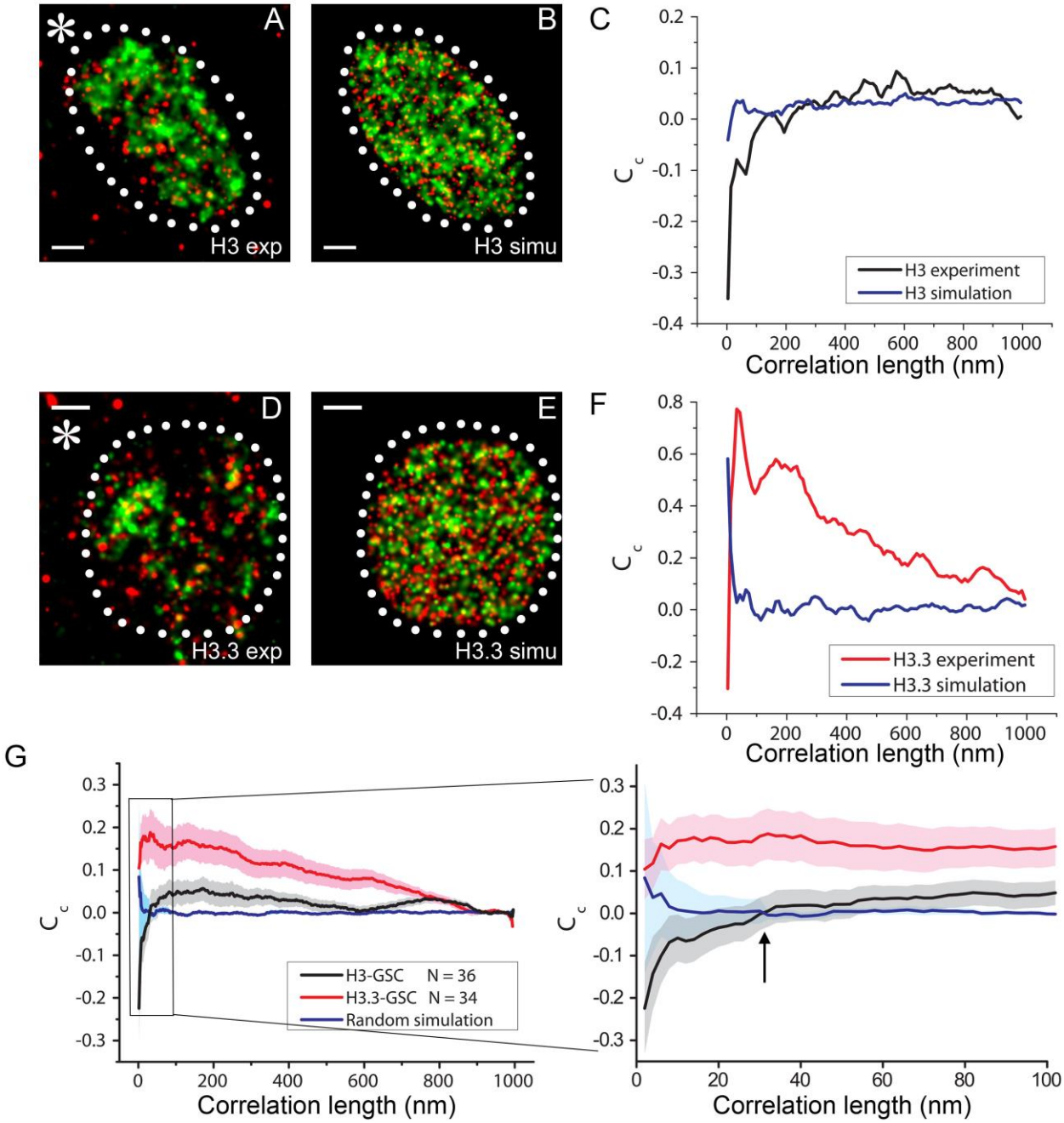

Figure 3: Distribution of H3/H3.3-Dronpa and H3/H3.3-PAmCherry in interphase GSCs using PALM. (**A**) A representative overlaid interphase GSC PALM image with H3-Dronpa (green) and H3-PAmCherry (red). (**B**) A simulated image using the same numbers of detected Dronpa and PAmCherry molecules randomly distributed on the same nucleus area as shown in (**A**). (**C**) Pairwise cross-correlation analysis of (**A**) and (**B**). (**D**) A representative overlaid

bioRxiv preprint doi: https://doi.org/10.1101/242768; this version posted January 4, 2018. The copyright holder for this preprint (which was not certified by peer review) is the author/funder. All rights reserved. No reuse allowed without permission.

interphase GSC PALM image with H3.3-Dronpa (green) and H3.3-PAmCherry (red). (**E**) A simulated image using the same numbers of detected Dronpa and PAmCherry molecules randomly distributed on the same nucleus area as shown in (**D**). (**F**) Cross-correlation analysis of (**D**) and (**E**). (**G**) Average cross-correlation curves show that the experimentally measured distributions of H3-Dronpa and H3-PAmCherry are anti-correlated below the length scale of ~ 32 nm (28-36nm, arrow in zoom-in view), which are significantly different from the uncorrelated simulated random distributions (blue curve) or correlated distributions of H3.3-Dronpa and H3.3-PAmCherry (red curve). Scale bar: 1μm. Asterisk: hub.

bioRxiv preprint doi: https://doi.org/10.1101/242768; this version posted January 4, 2018. The copyright holder for this preprint (which was not certified by peer review) is the author/funder. All rights reserved. No reuse allowed without permission.

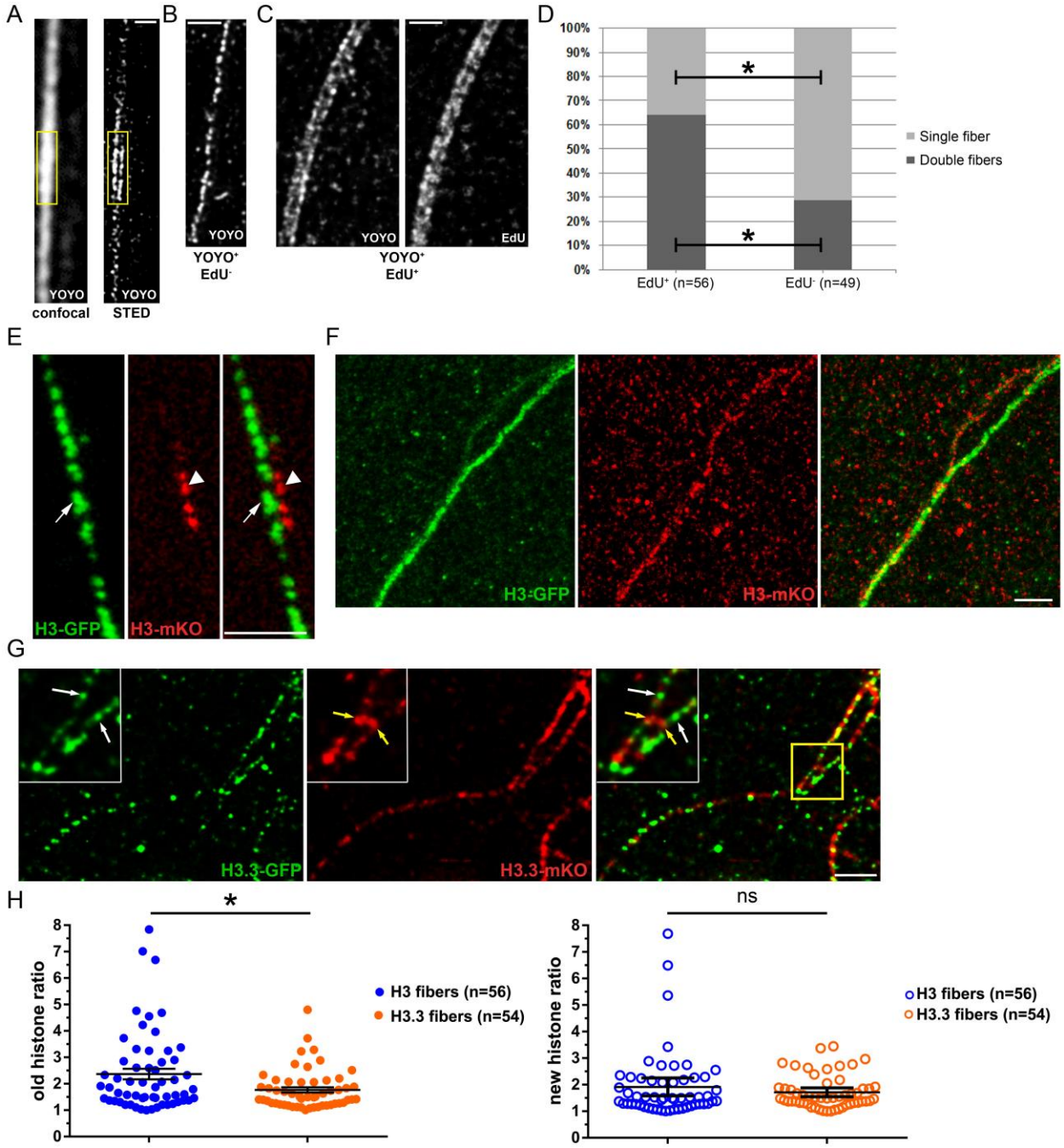

Figure 4: Distribution of H3/H3.3-GFP and H3/H3.3-mKO on chromatin fibers using STED imaging. (**A**) YOYO-3-labelled chromatin fiber visualized by confocal *versus* STED microscopy. Confocal image shows chromatin fiber with regions of variable brightness; low YOYO-3 intensity and high YOYO-3 intensity (boxed region). STED image shows regions of low YOYO-3 intensity in confocal image resolve into singlet fiber structure whereas high

bioRxiv preprint doi: https://doi.org/10.1101/242768; this version posted January 4, 2018. The copyright holder for this preprint (which was not certified by peer review) is the author/funder. All rights reserved. No reuse allowed without permission.

YOYO-3 intensity regions resolve into doublet fiber structure. (**B**) YOYO-3$^+$, EdU$^-$ fiber shows singlet fiber structure using STED imaging. (**C**) YOYO-3$^+$, EdU$^+$ fiber showing doublet fiber structure using STED imaging. (**D**) Quantification of singlet *versus* doublet fiber structure in EdU$^-$ *versus* EdU$^+$ fiber pools. Significantly more EdU$^-$ fibers are singlet whereas significantly more EdU$^+$ fibers are doublet. * $P< 0.05$, Chi-squared test. (**E**) STED image of H3-GFP (green) and H3-mKO (red)-labelled chromatin fibers shows a small region of new histone incorporation. Fiber shows singlet morphology except for the region where new H3-mKO (arrowhead) has been deposited at the opposite side from H3-GFP (arrow). (**F**) STED image of H3-GFP and H3-mKO labelled chromatin fiber shows a large region of new histone incorporation. H3-GFP is predominantly concentrated on one fiber whereas H3-mKO is largely concentrated on the other fiber. Doublet fibers show tight cohesion for a majority of the fiber length except for the breathing region where the two fibers show obvious separation. (**G**) STED image of H3.3-GFP and H3.3-mKO labelled chromatin fiber shows more even distribution of GFP and mKO signals between the doublet fibers. Insets: white arrows and yellow arrows pointed to symmetric old H3.3 and new H3.3 on sister chromatids, respectively. (**H**) Quantification of old histone (GFP) and new histone (mKO) ratios between two sides of the doublet fibers. * $P<0.05$ Mann-Whitney u test. Scale bar for (**A-C**): 500nm, for (**E-G**): 1μm.

bioRxiv preprint doi: https://doi.org/10.1101/242768; this version posted January 4, 2018. The copyright holder for this preprint (which was not certified by peer review) is the author/funder. All rights reserved. No reuse allowed without permission.

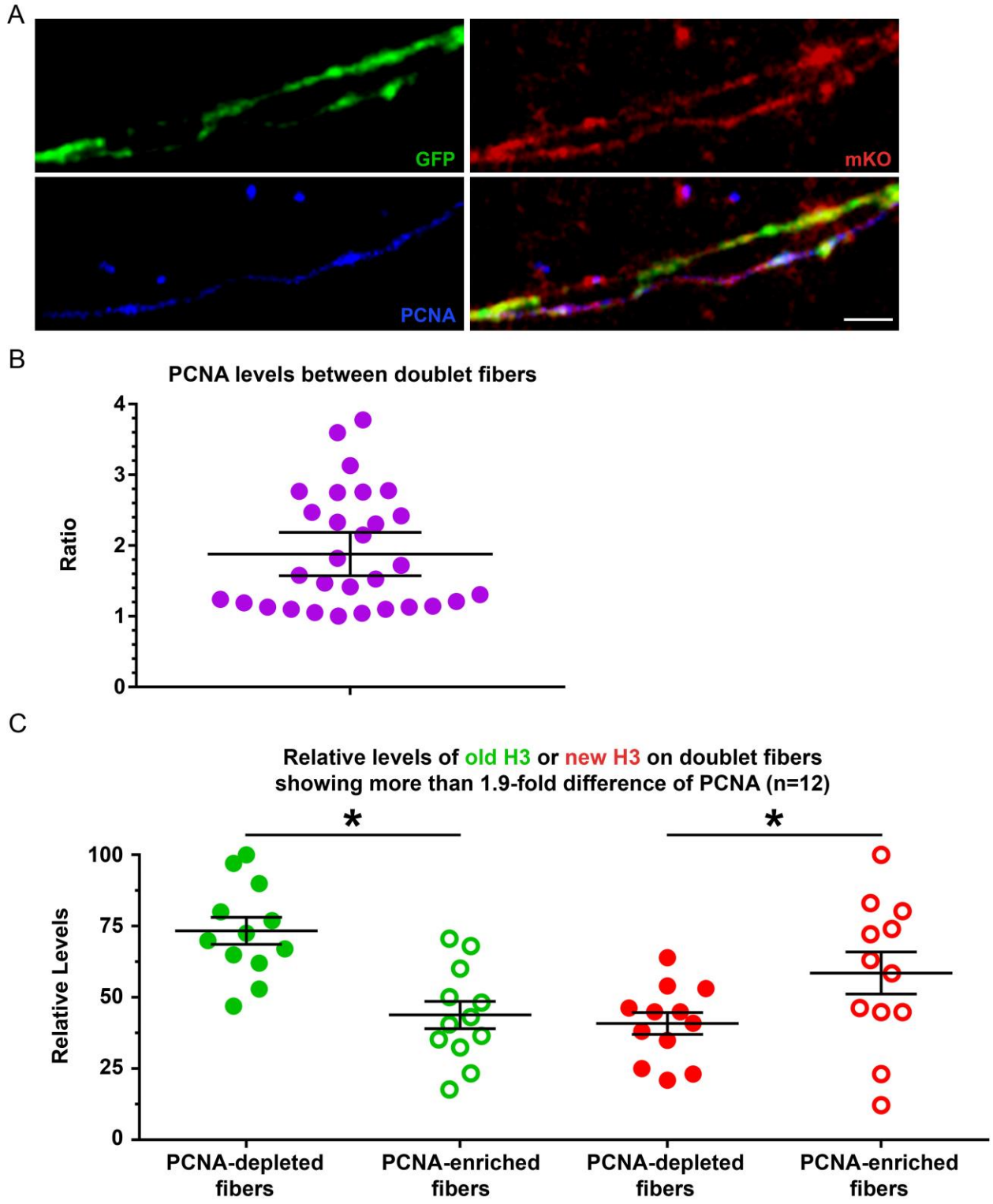

Figure 5: Distribution of H3-GFP and H3-mKO with lagging strand-enriched PCNA on chromatin fibers using STED imaging. (**A**) A representative doublet chromatin fiber shows old

bioRxiv preprint doi: https://doi.org/10.1101/242768; this version posted January 4, 2018. The copyright holder for this preprint (which was not certified by peer review) is the author/funder. All rights reserved. No reuse allowed without permission.

H3-GFP (green), new H3-mKO (red) and PCNA (blue). H3-GFP shows a relative depletion on the fiber stained with PCNA compared to H3-GFP signal on PCNA-depleted fiber. H3-mKO shows slight enrichment on PCNA-enriched fiber compared to H3-mKO levels on PCNA-depleted fiber. (**B**) Average ratio of PCNA levels enrichment between doublet chromatin fibers, quantified in 2μm unit. (**C**) Quantification of the relative levels of old H3-GFP (green) and new H3-mKO (red) in fibers units which show > 2-fold difference of PCNA levels between doublet fibers from (**B**). * $P<0.05$, Paired t-test for old H3 group (green dots and green circles), Mann-Whitney u test for new H3 group (red dots and red circles). Scale bar: 1μm.

bioRxiv preprint doi: https://doi.org/10.1101/242768; this version posted January 4, 2018. The copyright holder for this preprint (which was not certified by peer review) is the author/funder. All rights reserved. No reuse allowed without permission.

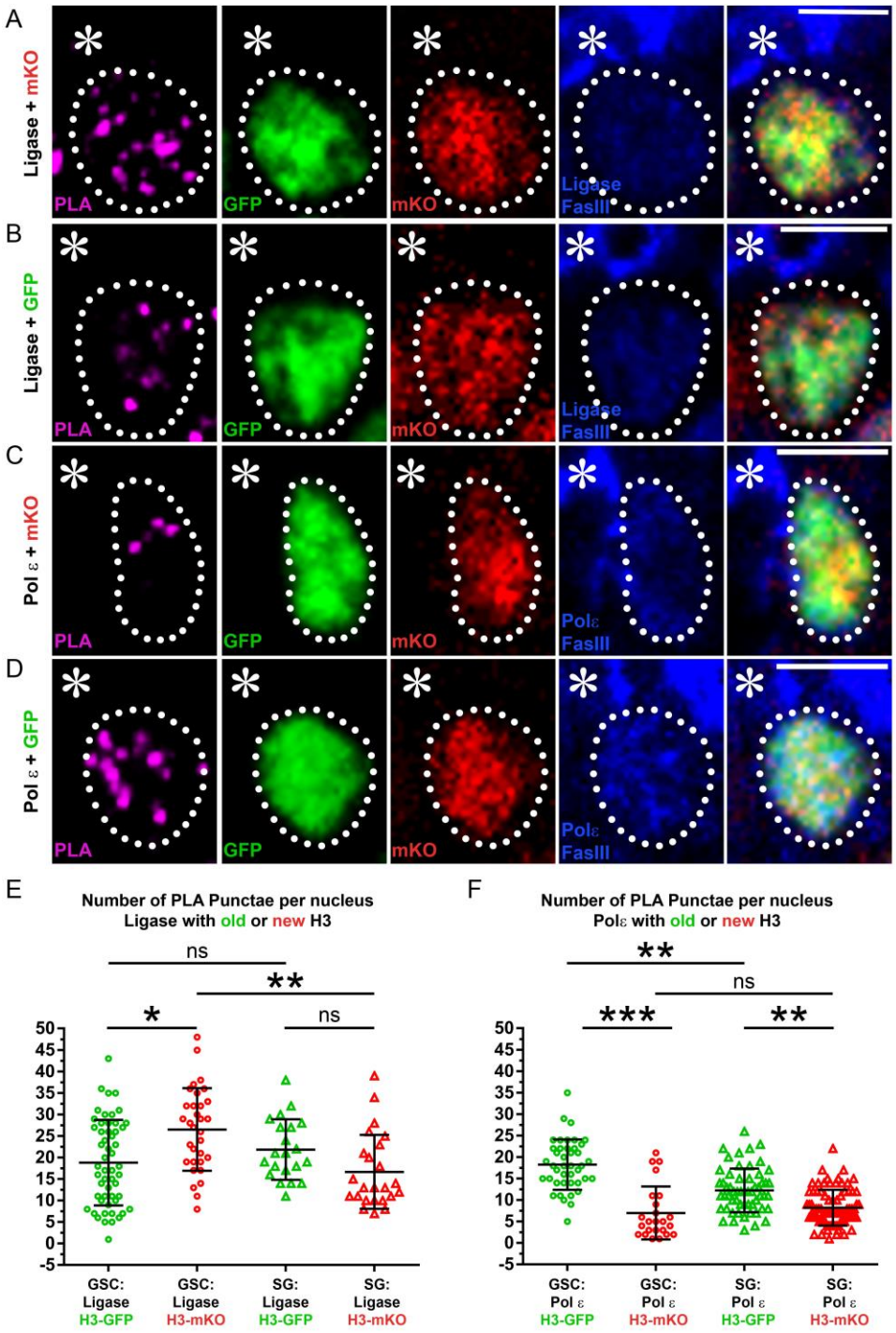

Figure 6: Proximity ligation assay shows distinct proximity between histones (old *versus* new) and different DNA replication machinery components (leading *versus* lagging) in GSCs and SGs. (**A**) A representative GSC showing PLA signals (magenta) between lagging-strand enriched Ligase-HA (blue) and new H3-mKO (red), old H3-GFP is in green. (**B**) A

bioRxiv preprint doi: https://doi.org/10.1101/242768; this version posted January 4, 2018. The copyright holder for this preprint (which was not certified by peer review) is the author/funder. All rights reserved. No reuse allowed without permission.

representative GSC showing PLA signals between Ligase-HA and old H3-GFP. (**C**) A representative GSC showing PLA signals between the leading-strand specific Polε-HA and new H3-mKO. (**D**) A representative GSC showing PLA signals between Polε-HA and old H3-GFP. (**E**) Quantification of the number of PLA puncta per nucleus between Ligase and histones (old *versus* new) in GSCs and SGs. (**F**) Quantification of the number of PLA puncta per nucleus between Polε and histones (old *versus* new) in GSCs and SGs. For GSCs: old histone shows more association with Pol ε than does new histone; new histone shows more association with Ligase than does old histone. For SGs: Old histone shows more association with Pol ε than does new histone; however, new histone shows indistinguishable association with Ligase compared to old histone. Old histone also shows more association with Pol ε in GSCs than in SGs, whereas old histone associates with Ligase indistinguishably in GSCs compared to SGs. New histone shows more association with Ligase in GSCs than in SGs, whereas new histone associates with Pol ε indistinguishably in GSCs compared to SGs. *: $P< 0.01$, **: $P< 0.001$, ***: $P< 0.0001$, Kruskal-Wallis multiple comparisons of non-parametric data with Dunn's multiple comparisons corrections test. Scale bar: 5μm.

bioRxiv preprint doi: https://doi.org/10.1101/242768; this version posted January 4, 2018. The copyright holder for this preprint (which was not certified by peer review) is the author/funder. All rights reserved. No reuse allowed without permission.

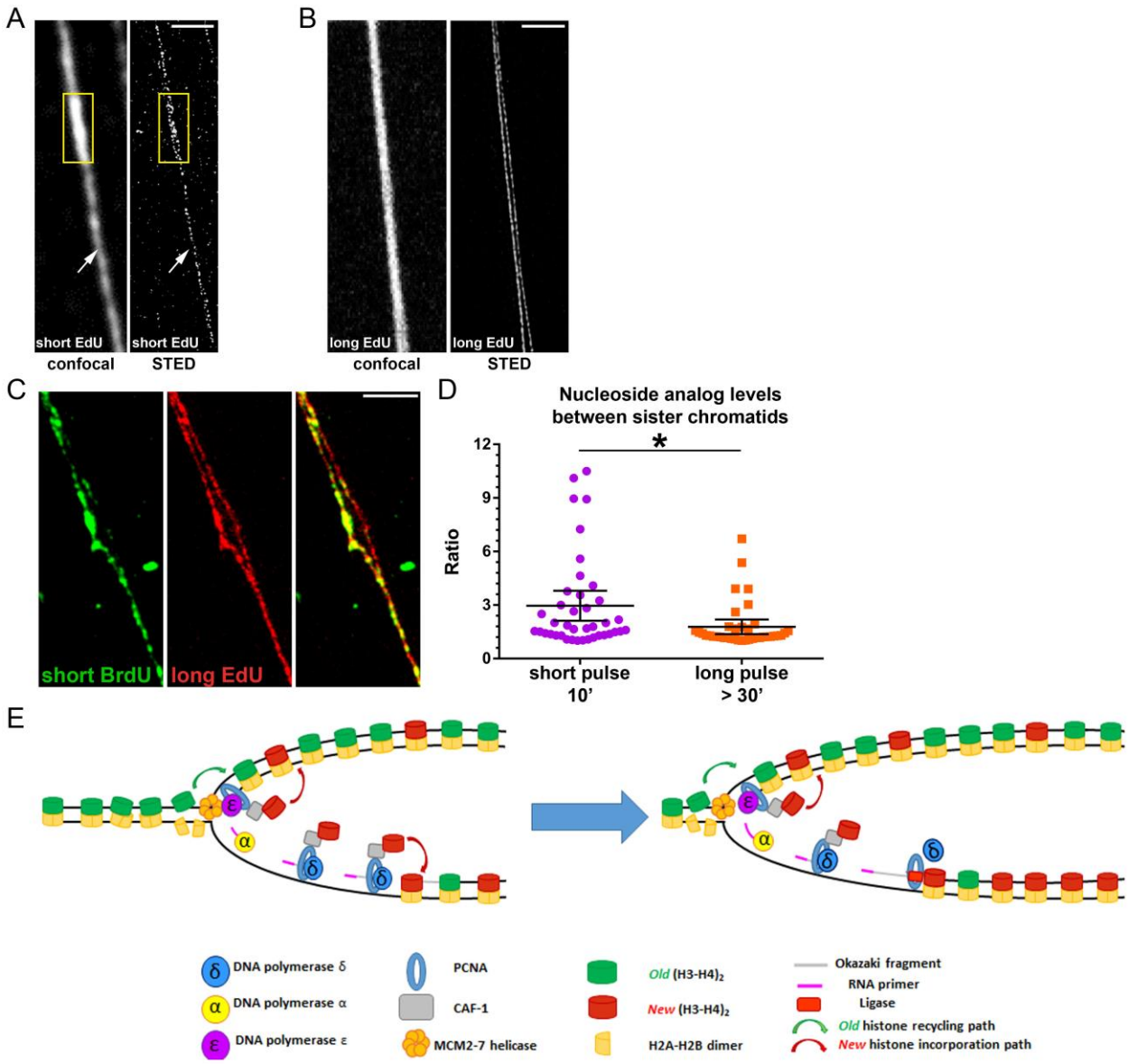

Figure 7: Replicating chromatin fiber show different timing of DNA replication. (**A**) Chromatin fibers labeled with short EdU pulse (10 minutes) visualized by confocal and STED imaging. (**B**) Chromatin fibers labeled with long EdU pulse (120 minutes) visualized by confocal and STED imaging. (**C**) Chromatin fibers labeled with dual-pulse with a short (10 minutes) BrdU (green) and a long (≥ 30 minutes) EdU (red) show more asymmetry in BrdU distribution between doublet sister fibers compared to EdU distribution between sister fibers (arrow and arrowhead point to the doublet sister fibers). Scale bar: 1μm. (**D**) Quantification of thymidine

bioRxiv preprint doi: https://doi.org/10.1101/242768; this version posted January 4, 2018. The copyright holder for this preprint (which was not certified by peer review) is the author/funder. All rights reserved. No reuse allowed without permission.

analogue asymmetry between doublet sister fibers with short (10 minutes) or long (≥ 30 min) pulses. Short pulse condition results in significantly more asymmetry in analogue distribution between doublet sister fibers than long pulse condition. * $P < 0.01$, Mann-Whitney Test. (**E**) A cartoon depicting asynchronous DNA replication and replication coupled nucleosome assembly: The leading strand is synthesized ahead of the lagging strand. Old histone is displaced and recycled onto the fully synthesized leading strand. Lagging strand replication eventually catches up with the leading strand, at which time new histone are largely incorporated to the lagging strand as recycled old histones have already been incorporated into the leading strand.

EXPERIMENTAL PROCEDURES

Chromatin fiber preparation with nucleoside analogue incorporation and immunostaining

Wandering third-instar larvae were dissected in room temperature Schneider's medium to isolate *Drosophila* testis. Testis were subsequently moved into Schneider's media containing 100uM concentration EdU analogue and incubated for desired time (10, 30 or 120) minutes. For dual-labelling experiments: Schneider's media containing EdU was drained and replaced with media containing 100uM BrdU analogue and incubated for 10 minutes. BrdU/EdU-containing media was drained and replaced with Dulbecco's PBS containing Mg^{2+} and Ca^{2+} as well as 1% formaldehyde and incubated for 1 minute. Testis were drained of fixative and washed in 1X Dulbecco's PBS containing Mg^{2+} and Ca^{2+}. Following wash, testis were incubated in Dulbecco's PBS with Mg^{2+} and $Ca^{2+}$with collagenase/dispase added to a final concentration of 2mg/ml Testis were incubated in a 37°Cwater bath for 15 minutes. Slides for cytospin centrifuge were prepared using guidelines provided in manual (Cytospin™ 3 Manual). 500ul of dissociated testis cell suspension were then pipetted into cytospin funnels to deposit cells on glass surface, slides

bioRxiv preprint doi: https://doi.org/10.1101/242768; this version posted January 4, 2018. The copyright holder for this preprint (which was not certified by peer review) is the author/funder. All rights reserved. No reuse allowed without permission.

were loaded into Cytospin 3™ and spun at 900 rpms for 4 minutes. Following centrifugation, cells were placed in 50ml conical containing 50 ml of lysis buffer (500mM NaCl; 500mM Urea, 25mM Tris, 1% Triton, pH 7.5) (Note: 50ml conical contained a small hole placed in the bottom with a 20 gauge hypodermic needle to allow for steady removal of lysis buffer during fiber stretching). Cells were incubated for 15 minutes. (Note: the cap of conical tube was placed on top to prevent lysis buffer from flowing out during lysis incubation.) After 15 minutes, the cap on the 50ml conical tube was loosened to allow lysis buffer to flow out slowly. Slides were removed from tubes and placed on a flat surface, after which 1mL fixative solution was added (1ml PBS with 4% formaldehyde) slowly to the top of the slide, above where the cells have been deposited. Slides were incubated for 10 minutes after which fixative solution was removed and cells were washed for 30 minutes in Copeland jar containing 50ul room temperature PBS after which antibody stain was performed as specified previously. Note: For BrdU: Fibers were treated with 1M HCL for 1hr at 37°C to expose BrdU epitope prior to addition of anti-BrdU primary antibody. For EdU visualization: EdU analogue was conjugated to alexa-647 dye via CLICK chemistry [reviewed by (Kolb et al., 2001; Moses and Moorhouse, 2007)].

Superresolution STED imaging

Superresolution images were acquired using a Leica TCS SP8 STED microscope with a 1.4 NA 100X STED White objective. Antibody staining enhanced specimen brightness and photostability for STED. Secondary antibody fluorophore conjugates were empirically selected for STED performance and optimal 3-colour separation with the 592 nm continuous wave (CW) and 775 nm pulsed depletion lasers (Alexa 488 with STED 592nm, Alexa 568 with STED 775nm, and Alexa 647 with STED 775nm). Images were acquired as single z-planes for all

bioRxiv preprint doi: https://doi.org/10.1101/242768; this version posted January 4, 2018. The copyright holder for this preprint (which was not certified by peer review) is the author/funder. All rights reserved. No reuse allowed without permission.

tissue types; whole mount, squash and fiber preparations to minimize drift between channel acquisitions. Specimens included 100 nm TetraSpeck microsphere beads as fiducial markers (Thermo Fisher Catalog No. T7279). Instrument aberration and blurring was corrected with post-acquisition deconvolution using the Scientific Volume Imagine (SVI) Huygens Professional software package, which achieves improved calculated/theoretical PSFs via complete integration with the Leica LAS-X software and hardware. Detailed instrument acquisition and post-processing settings are available upon request.

PLA Assay

Following incubation with primary antibodies, proximity ligation assay (PLA; Olink) was performed using 20 µL of reaction per step per slide according to Sigma-Aldrich® Duolink® In Situ PLA® manufacturer's instruction. In brief, two PLA secondary probes, anti-mouse MINUS (targeting anti-HA mouse primary) and anti-rabbit PLUS (targeting anti-GFP or anti-mKO rabbit primaries), were diluted 1:5 in Ab Diluent buffer provided by manufacturer and incubated overnight at 4 °C. Slides were washed in 1X wash buffer A for 10 minutes, followed by the ligation reaction, in which PLA ligation stock was diluted 1:5 in dH_2O and 1:40 ligase was added and incubated for 1hr at 37 °C. Slides were washed in wash buffer A for 5 minutes, followed by addition of the PLA amplification reaction (1:5 amplification stock and 1:80 polymerase diluted in dH_2O) covered for 2 hours at 37 °C. Slides were washed with 1X wash buffer B for 10 mins and 0.01X wash buffer B for 1 minute. Slides were then washed once in 1X PBS. Anti-mouse secondary was added (Alexa Fluor 405; 1:1000 Molecular Probes®) Images were taken using the Zeiss LSM 700 Multiphoton confocal

bioRxiv preprint doi: https://doi.org/10.1101/242768; this version posted January 4, 2018. The copyright holder for this preprint (which was not certified by peer review) is the author/funder. All rights reserved. No reuse allowed without permission.

microscope with a 63× oil immersion objectives and processed using Adobe Photoshop software.

AUTHOR CONTRIBUTIONS

Conceptualization, M.W., Z.N., X.Y., J.S., R.R., J.G., J.X. and X.C.; Methodology, M.W., Z.N., X.Y., J.S., R.R., J.G., J.X., and X.C.; Investigation, M.W., Z.N., X.Y., J.S., R.R., J-M. K., E.U., V.T., J.B.; Writing – Original Draft, M.W., Z.N., X.Y., J.S., R.R., J.G., J.X. and X.C.; Funding Acquisition, J.X., J.G. and X.C.; Supervision, J.X., J.G. and X.C.

ACKNOWLEDGMENTS

We thank E. Moudrianakis, A. Spradling, J. Berger, M. Van Doren, R. Johnston and X.C. lab members for suggestions. We thank Johns Hopkins Integrated Imaging Center for confocal imaging and Carnegie Institute Imaging Center for STED microscopy work. Supported by NIH 5T32GM007231 and F31 GM115149-01A1 (M.W.), NIH R01GM112008 (J.X.), NIH R01 GM33397 (J.G.), NIH R01GM112008, the Howard Hughes Medical Institute, the Bill & Melinda Gates Foundation, the Simons Foundation, the David and Lucile Packard Foundation, and Johns Hopkins University startup funds (X.C.)

bioRxiv preprint doi: https://doi.org/10.1101/242768; this version posted January 4, 2018. The copyright holder for this preprint (which was not certified by peer review) is the author/funder. All rights reserved. No reuse allowed without permission.

REFERENCES

Adkins, N.L., Swygert, S.G., Kaur, P., Niu, H., Grigoryev, S.A., Sung, P., Wang, H., and Peterson, C.L. (2017). Nucleosome-like, Single-stranded DNA (ssDNA)-Histone Octamer Complexes and the Implication for DNA Double Strand Break Repair. Journal of Biological Chemistry *292*, 5271-5281.

Ahmad, K., and Henikoff, S. (2002a). Histone H3 variants specify modes of chromatin assembly. Proc Natl Acad Sci U S A *99 Suppl 4*, 16477-16484.

Ahmad, K., and Henikoff, S. (2002b). The histone variant H3.3 marks active chromatin by replication-independent nucleosome assembly. Mol Cell *9*, 1191-1200.

Alabert, C., Barth, T.K., Reverón-Gómez, N., Sidoli, S., Schmidt, A., Jensen, O.N., Imhof, A., and Groth, A. (2015). Two distinct modes for propagation of histone PTMs across the cell cycle. Genes & Development *29*, 585-590.

Alabert, C., and Groth, A. (2012). Chromatin replication and epigenome maintenance. Nat Rev Mol Cell Biol *13*, 153-167.

Alberts, B.M., Barry, J., Bedinger, P., Formosa, T., Jongeneel, C.V., and Kreuzer, K.N. (1983). Studies on DNA replication in the bacteriophage T4 in vitro system. Cold Spring Harb Symp Quant Biol *47 Pt 2*, 655-668.

Allis, C.D., and Jenuwein, T. (2016). The molecular hallmarks of epigenetic control. Nat Rev Genet *17*, 487-500.

Annunziato, A.T. (2013). Assembling chromatin: the long and winding road. Biochim Biophys Acta *1819*, 196-210.

Annunziato, A.T., Schindler, R.K., Riggs, M.G., and Seale, R.L. (1982). Association of newly synthesized histones with replicating and nonreplicating regions of chromatin. J Biol Chem *257*, 8507-8515.

Atlasi, Y., and Stunnenberg, H.G. (2017). The interplay of epigenetic marks during stem cell differentiation and development. Nat Rev Genet *18*, 643-658.

Avgustinova, A., and Benitah, S.A. (2016). Epigenetic control of adult stem cell function. Nat Rev Mol Cell Biol *17*, 643-658.

Balakrishnan, L., and Bambara, R.A. (2013). Okazaki Fragment Metabolism. Cold Spring Harbor Perspectives in Biology *5*.

Bermek, O., Willcox, S., and Griffith, J.D. (2015). DNA Replication Catalyzed by Herpes Simplex Virus Type 1 Proteins Reveals Trombone Loops at the Fork. J Biol Chem *290*, 2539-2545.

Bessman, M.J., Kornberg, A., Lehman, I.R., and Simms, E.S. (1956). Enzymic synthesis of deoxyribonucleic acid. Biochimica et biophysica acta *21*, 197-198.

Bessman, M.J., Lehman, I.R., Simms, E.S., and Kornberg, A. (1958). Enzymatic synthesis of deoxyribonucleic acid. II. General properties of the reaction. The Journal of biological chemistry *233*, 171-177.

Betschinger, J., and Knoblich, J.A. (2004). Dare to be different: asymmetric cell division in Drosophila, C. elegans and vertebrates. Curr Biol *14*, R674-685.

Betzig, E., Patterson, G.H., Sougrat, R., Lindwasser, O.W., Olenych, S., Bonifacino, J.S., Davidson, M.W., Lippincott-Schwartz, J., and Hess, H.F. (2006). Imaging intracellular fluorescent proteins at nanometer resolution. Science *313*, 1642-1645.

Blower, M.D., Sullivan, B.A., and Karpen, G.H. (2002). Conserved Organization of Centromeric Chromatin in Flies and Humans. Developmental Cell *2*, 319-330.

bioRxiv preprint doi: https://doi.org/10.1101/242768; this version posted January 4, 2018. The copyright holder for this preprint (which was not certified by peer review) is the author/funder. All rights reserved. No reuse allowed without permission.

Burgess, R.J., and Zhang, Z. (2013). Histone chaperones in nucleosome assembly and human disease. Nat Struct Mol Biol *20*, 14-22.
Clevers, H. (2005). Stem cells, asymmetric division and cancer. Nat Genet *37*, 1027-1028.
Cohen, S.M., Chastain, P.D., 2nd, Cordeiro-Stone, M., and Kaufman, D.G. (2009). DNA replication and the GINS complex: localization on extended chromatin fibers. Epigenetics Chromatin *2*, 6.
Debyser, Z., Tabor, S., and Richardson, C.C. (1994). Coordination of leading and lagging strand DNA synthesis at the replication fork of bacteriophage T7. Cell *77*, 157-166.
Dunn, K., and Griffith, J.D. (1980). The presence of RNA in a double helix inhibits its interaction with histone protein. Nucleic Acids Res *8*, 555-566.
Fuller, M.T., and Spradling, A.C. (2007). Male and female Drosophila germline stem cells: two versions of immortality. Science *316*, 402-404.
Graham, J.E., Marians, K.J., and Kowalczykowski, S.C. (2017). Independent and Stochastic Action of DNA Polymerases in the Replisome. Cell *169*, 1201-1213 e1217.
Hamdan, S.M., Loparo, J.J., Takahashi, M., Richardson, C.C., and van Oijen, A.M. (2009). Dynamics of DNA replication loops reveal temporal control of lagging-strand synthesis. Nature *457*, 336-339.
Hell, S.W., and Wichmann, J. (1994). Breaking the diffraction resolution limit by stimulated emission: stimulated-emission-depletion fluorescence microscopy. Opt Lett *19*, 780-782.
Horvath, P., and Barrangou, R. (2010). CRISPR/Cas, the immune system of bacteria and archaea. Science *327*, 167-170.
Inaba, M., and Yamashita, Y.M. (2012). Asymmetric stem cell division: precision for robustness. Cell Stem Cell *11*, 461-469.
Jackson, V. (1988). Deposition of newly synthesized histones: hybrid nucleosomes are not tandemly arranged on daughter DNA strands. Biochemistry *27*, 2109-2120.
Jackson, V., and Chalkley, R. (1981a). A new method for the isolation of replicative chromatin: selective deposition of histone on both new and old DNA. Cell *23*, 121-134.
Jackson, V., and Chalkley, R. (1981b). A reevaluation of new histone deposition on replicating chromatin. J Biol Chem *256*, 5095-5103.
Jackson, V., and Chalkley, R. (1985). Histone segregation on replicating chromatin. Biochemistry *24*, 6930-6938.
Kadyrov, F.A., and Drake, J.W. (2002). Characterization of DNA synthesis catalyzed by bacteriophage T4 replication complexes reconstituted on synthetic circular substrates. Nucleic Acids Research *30*, 4387-4397.
Katan-Khaykovich, Y., and Struhl, K. (2011). Splitting of H3-H4 tetramers at transcriptionally active genes undergoing dynamic histone exchange. Proc Natl Acad Sci U S A *108*, 1296-1301.
Kimura, H. (2005). Histone dynamics in living cells revealed by photobleaching. DNA Repair (Amst) *4*, 939-950.
Kolb, H.C., Finn, M.G., and Sharpless, K.B. (2001). Click Chemistry: Diverse Chemical Function from a Few Good Reactions. Angew Chem Int Ed Engl *40*, 2004-2021.
Kornberg, A., Lehman, I.R., Bessman, M.J., and Simms, E.S. (1989). Enzymic synthesis of deoxyribonucleic acid. 1956. Biochimica et biophysica acta *1000*, 57-58.
Kouzarides, T. (2007). Chromatin modifications and their function. Cell *128*, 693-705.
Lee, J., Chastain, P.D., Kusakabe, T., Griffith, J.D., and Richardson, C.C. (1998). Coordinated Leading and Lagging Strand DNA Synthesis on a Minicircular Template. Molecular Cell *1*, 1001-1010.

bioRxiv preprint doi: https://doi.org/10.1101/242768; this version posted January 4, 2018. The copyright holder for this preprint (which was not certified by peer review) is the author/funder. All rights reserved. No reuse allowed without permission.

Lee, J.B., Hite, R.K., Hamdan, S.M., Xie, X.S., Richardson, C.C., and van Oijen, A.M. (2006). DNA primase acts as a molecular brake in DNA replication. Nature *439*, 621-624.
Leffak, I.M., Grainger, R., and Weintraub, H. (1977). Conservative assembly and segregation of nucleosomal histones. Cell *12*, 837-845.
Lehman, I.R., Bessman, M.J., Simms, E.S., and Kornberg, A. (1958). Enzymatic synthesis of deoxyribonucleic acid. I. Preparation of substrates and partial purification of an enzyme from Escherichia coli. The Journal of biological chemistry *233*, 163-170.
Liu, Y., Giannopoulou, E.G., Wen, D., Falciatori, I., Elemento, O., Allis, C.D., Rafii, S., and Seandel, M. (2016). Epigenetic profiles signify cell fate plasticity in unipotent spermatogonial stem and progenitor cells. Nature Communications *7*, 11275.
McKnight, S.L., and Miller, O.L., Jr. (1977). Electron microscopic analysis of chromatin replication in the cellular blastoderm Drosophila melanogaster embryo. Cell *12*, 795-804.
Morrison, S.J., and Kimble, J. (2006). Asymmetric and symmetric stem-cell divisions in development and cancer. Nature *441*, 1068-1074.
Moses, J.E., and Moorhouse, A.D. (2007). The growing applications of click chemistry. Chemical Society reviews *36*, 1249-1262.
Nieminuszczy, J., Schwab, R.A., and Niedzwiedz, W. (2016). The DNA fibre technique – tracking helicases at work. Methods *108*, 92-98.
Okazaki, R., Okazaki, T., Sakabe, K., Sugimoto, K., and Sugino, A. (1968). Mechanism of DNA chain growth. I. Possible discontinuity and unusual secondary structure of newly synthesized chains. Proceedings of the National Academy of Sciences of the United States of America *59*, 598-605.
Petruk, S., Sedkov, Y., Johnston, D.M., Hodgson, J.W., Black, K.L., Kovermann, S.K., Beck, S., Canaani, E., Brock, H.W., and Mazo, A. (2012). TrxG and PcG proteins but not methylated histones remain associated with DNA through replication. Cell *150*, 922-933.
Prelich, G., and Stillman, B. (1988). Coordinated leading and lagging strand synthesis during SV40 DNA replication in vitro requires PCNA. Cell *53*, 117-126.
Riley, D., and Weintraub, H. (1979). Conservative segregation of parental histones during replication in the presence of cycloheximide. Proc Natl Acad Sci U S A *76*, 328-332.
Roufa, D.J., and Marchionni, M.A. (1982). Nucleosome segregation at a defined mammalian chromosomal site. Proc Natl Acad Sci U S A *79*, 1810-1814.
Russev, G., and Hancock, R. (1981). Formation of hybrid nucleosomes cantaining new and old histones. Nucleic Acids Res *9*, 4129-4137.
Rust, M.J., Bates, M., and Zhuang, X. (2006). Sub-diffraction-limit imaging by stochastic optical reconstruction microscopy (STORM). Nat Methods *3*, 793-795.
Sakabe, K., and Okazaki, R. (1966). A unique property of the replicating region of chromosomal DNA. Biochimica et biophysica acta *129*, 651-654.
Seale, R.L. (1976). Studies on the mode of segregation of histone nu bodies during replication in HeLa cells. Cell *9*, 423-429.
Seidman, M.M., Levine, A.J., and Weintraub, H. (1979). The asymmetric segregation of parental nucleosomes during chrosome replication. Cell *18*, 439-449.
Sheng, X.R., and Matunis, E. (2011). Live imaging of the Drosophila spermatogonial stem cell niche reveals novel mechanisms regulating germline stem cell output. Development *138*, 3367-3376.
Snedeker, J., Wooten, M., and Chen, X. (2017). The Inherent Asymmetry of DNA Replication. Annu Rev Cell Dev Biol *33*, 291-318.

bioRxiv preprint doi: https://doi.org/10.1101/242768; this version posted January 4, 2018. The copyright holder for this preprint (which was not certified by peer review) is the author/funder. All rights reserved. No reuse allowed without permission.

Sogo, J.M., Stahl, H., Koller, T., and Knippers, R. (1986). Structure of replicating simian virus 40 minichromosomes. The replication fork, core histone segregation and terminal structures. J Mol Biol *189*, 189-204.
Stano, N.M., Jeong, Y.J., Donmez, I., Tummalapalli, P., Levin, M.K., and Patel, S.S. (2005). DNA synthesis provides the driving force to accelerate DNA unwinding by a helicase. Nature *435*, 370-373.
Stengel, G., and Kuchta, R.D. (2011). Coordinated Leading and Lagging Strand DNA Synthesis by Using the Herpes Simplex Virus 1 Replication Complex and Minicircle DNA Templates. J Virol *85*, 957-967.
Tran, V., Feng, L., and Chen, X. (2013). Asymmetric distribution of histones during Drosophila male germline stem cell asymmetric divisions. Chromosome Res *21*, 255-269.
Tran, V., Lim, C., Xie, J., and Chen, X. (2012). Asymmetric division of Drosophila male germline stem cell shows asymmetric histone distribution. Science *338*, 679-682.
Van Doren, M., Williamson, A.L., and Lehmann, R. (1998). Regulation of zygotic gene expression in Drosophila primordial germ cells. Curr Biol *8*, 243-246.
Veatch, S.L., Machta, B.B., Shelby, S.A., Chiang, E.N., Holowka, D.A., and Baird, B.A. (2012). Correlation functions quantify super-resolution images and estimate apparent clustering due to over-counting. PLoS One *7*, e31457.
Verreault, A. (2003). Histone Deposition at the Replication Fork: A Matter of Urgency. Molecular Cell *11*, 283-284.
Watson, J.D., and Crick, F.H.C. (1953). Molecular Structure of Nucleic Acids: A Structure for Deoxyribose Nucleic Acid. Nature *171*, 737-738.
Weintraub, H. (1976). Cooperative alignment of nu bodies during chromosome replication in the presence of cycloheximide. Cell *9*, 419-422.
Worcel, A., Han, S., and Wong, M.L. (1978). Assembly of newly replicated chromatin. Cell *15*, 969-977.
Wright, A.V., Nunez, J.K., and Doudna, J.A. (2016). Biology and Applications of CRISPR Systems: Harnessing Nature's Toolbox for Genome Engineering. Cell *164*, 29-44.
Xie, J., Wooten, M., Tran, V., Chen, B.C., Pozmanter, C., Simbolon, C., Betzig, E., and Chen, X. (2015). Histone H3 Threonine Phosphorylation Regulates Asymmetric Histone Inheritance in the Drosophila Male Germline. Cell *163*, 920-933.
Xie, J., Wooten, M., Tran, V., and Chen, X. (2017). Breaking Symmetry - Asymmetric Histone Inheritance in Stem Cells. Trends Cell Biol *27*, 527-540.
Xu, M., Long, C., Chen, X., Huang, C., Chen, S., and Zhu, B. (2010). Partitioning of histone H3-H4 tetramers during DNA replication-dependent chromatin assembly. Science *328*, 94-98.
Yadlapalli, S., Cheng, J., and Yamashita, Y.M. (2011). Drosophila male germline stem cells do not asymmetrically segregate chromosome strands. J Cell Sci *124*, 933-939.
Yadlapalli, S., and Yamashita, Y.M. (2013). Chromosome-specific nonrandom sister chromatid segregation during stem-cell division. Nature.
Yang, J., Nelson, S.W., and Benkovic, S.J. (2006). The Control Mechanism for Lagging Strand Polymerase Recycling during Bacteriophage T4 DNA Replication. Molecular Cell *21*, 153-164.
Yao, N.Y., Georgescu, R.E., Finkelstein, J., and O'Donnell, M.E. (2009). Single-molecule analysis reveals that the lagging strand increases replisome processivity but slows replication fork progression. Proc Natl Acad Sci U S A *106*, 13236-13241.
Yeeles, Joseph T.P., and Marians, Kenneth J. Dynamics of Leading-Strand Lesion Skipping by the Replisome. Molecular Cell *52*, 855-865.

bioRxiv preprint doi: https://doi.org/10.1101/242768; this version posted January 4, 2018. The copyright holder for this preprint (which was not certified by peer review) is the author/funder. All rights reserved. No reuse allowed without permission.

Young, N.L., DiMaggio, P.A., and Garcia, B.A. (2010). The significance, development and progress of high-throughput combinatorial histone code analysis. Cellular and Molecular Life Sciences *67*, 3983-4000.

Yu, C., Gan, H., Han, J., Zhou, Z.X., Jia, S., Chabes, A., Farrugia, G., Ordog, T., and Zhang, Z. (2014). Strand-specific analysis shows protein binding at replication forks and PCNA unloading from lagging strands when forks stall. Mol Cell *56*, 551-563.